DIFFRACTION EFFECTS IN COHERENT TRANSITION RADIATION DIAGNOSTICS FOR SUB-MM BUNCH LENGTH MEASUREMENT*

T. J. Maxwell, D. Mihalcea, Northern Illinois University, DeKalb, IL 60115, U.S.A.
P. Piot, Northern Illinois University, DeKalb, IL 60115, and Fermilab, Batavia, IL 60510, U.S.A.

Abstract

Electrons crossing the boundary between different media generate bursts of transition radiation. In the case of bunches of N electrons, the radiation is coherent and has an N-squared enhancement at wavelengths related to the longitudinal bunch distribution. This coherent transition radiation has therefore attracted attention as an interceptive charged particle beam diagnostic technique. Many analytical descriptions have been devised describing the spectral distribution generated by electron bunches colliding with thin metallic foils making different simplifying assumptions. For typical bunches having lengths in the sub-millimeter range, measurable spectra are generated up into the millimeter range. Analysis of this THz radiation is performed using optical equipment tens of millimeters in size. This gives rise to concern that optical diffraction effects may spread the wavefront of interest into regions larger than the optical elements and partially escape detection, generating a wavelength-dependent instrument response. In this paper we present a model implementing vector diffraction theory to analyze these effects in bunch length diagnostics based on coherent transition radiation.

INTRODUCTION

Relativistic electrons impinging on a metallic foil emit transition radiation (TR) as they move from one medium to the next. In the case where a bunch of electrons is incident on the foil, the slight time delay in the arrival of the charges at the foil introduces a phase delay between emission of this TR. Summing contributions to the emitted electromagnetic radiation of the individual charges over the length of the bunch, one finds for the emitted radiation spectrum

$$I(\omega) = N^2 I_e(\omega) f(\omega) \qquad (1)$$

Here N is the number of charges in the bunch and $I_e(\omega)$ is the power spectrum for single electron TR. We assume N to be very large and leave in explicit dependence of the emitted TR spectrum on frequency. The last term $f(\omega)$ is referred to as the form factor of the bunch. For highly relativistic bunches under a one-dimensional line charge assumption, this is given roughly by

$$f(\omega) = \left| \int \rho_{long}(t) \exp(i\omega t) \right|^2 \qquad (2)$$

In principle, this N-squared-enhanced coherent transition radiation (CTR) provides a signal strong enough to detect for sufficient bunch charge. However, analysis of the CTR spectrum emitted by beams with typical bunch lengths σ_z on the order of hundreds of micrometers, one must also consider the possibility of diffraction losses in any optical system used for spectral analysis due to the long coherence wavelengths. The goal of this research is to determine the response function $R(\omega)$ of such optical systems and the single-electron TR frequency dependency such that one can correct the modified equation

$$I_{Measured}(\omega) = N^2 I_e(\omega) f(\omega) R(\omega) \qquad (3)$$

to recover the mod-squared Fourier transform of the longitudinal bunch distribution $f(\omega)$ from the measured signal.

SIMULATION

Extending previous work [1, 2] our approach is based on simulating ideal wavefront generation and propagation. Our model treats the radiation emitted at TR generation as the exact reflection of the relativistic electron's light-like electromagnetic field from the surface of the foil to generate $\vec{E}_e(\omega)$. At present the foil is treated as an ideal reflector, neglecting dielectric properties. Another approach to ensure proper treatment of the near-field electromagnetic radiation emission for low-energy electrons has been recently suggested in [3].

This source electromagnetic wave is then propagated through the optical system from one surface to the next using a fully three-dimensional vector diffraction integral as derived in [4]. While computationally expensive, this approach has demonstrated great accuracy over a wide variety of aperture size, diffraction distance, and wavelength ranges while preserving the detailed information necessary for reflections off of complex three-dimensional surfaces such as parabolic mirrors. Other methods have been suggested for accounting for these near-field phenomena via fast Fourier transform [5].

In taking this brute force approach to solving the diffraction problem, several enhancements have been added. The entire code is written in C++ and currently operates in a parallelized MPICH2 implementation. To work around the difficulty integrating over the electron's cusped source function in particular, the Cuba 1.4 [6] integration package has been added. Using Cuba's Cuhre adaptive cubature integrating routine, precision control over source integration to fix the overall energy scale of emitted TR wavefronts has been achieved and are in agreement with values predicted elsewhere [5].

Various benchmarks have been performed including comparison to other near-field ($D < \lambda \gamma^2$) TR predictions

*Work supported by US. Department of Energy, under Contract No. DE-FG02-06ER41435 with Northern Illinois University

and other basic diffraction patterns, some of which are outlined in [1]. Testing of repeated application of the diffraction integral as it is used in transporting the wavefront from one surface to the next has also been performed, tightly fixing constraints on the highest frequency that can be analyzed with reasonable accuracy.

SINGLE ELECTRON TRANSITION RADIATION

Further dissection the terms of Equation 3, we present simulated results of single-electron transition radiation as they pertain to the $I_e(\omega)$ term. TR simulations were done for radiation generated by γ = 50, 100, 500 and 2000 single electrons impinging at normal incidence with a 2" (50.8 mm) diameter foil. As shown in the literature, the emitted TR emanates in rings from the foil in the near field with the central ring having the greatest intensity. After reaching the TR formation length of $\lambda\gamma^2$, the radiation appears as a bright ring along a cone of opening angle $1/\gamma$.

The contour plot of Figure 1 (top) for γ = 100 shows the angular spectral fluence profiles with respect to frequency (horizontal axis) and the polar angle θ measured from the foil's normal (vertical axis). This was evaluated across a sphere of radius 50.8 mm. It has been previously noted [1] that the distribution takes a different form depending on the distance from the foil used to evaluate the TR wavefront. Changing the incident electron energy has shown only a change in the value of peak intensities with no change in the shape of the wavefronts. Integrating the resulting spectral fluence profiles for all the data over the entire half-sphere solid angle in the reflected back plane gives the resulting power spectra shown in Figure 1 (bottom).

The resulting power spectra given in Figure 1, bottom, demonstrate the diffraction limitations of the foil itself. All spectra plateau at $\nu = \gamma c / 3a$, where a is the radius of the foil, in agreement with [5]. For investigation of emitted CTR spectra at frequencies below this, the low-frequency TR suppression must be taken into account.

DIAGNOSTIC SYSTEM RESPONSE

The final component of Equation 3 to consider is any diffraction suppression due to partial acceptance of the diagnostic system's optics. As an example of such an effect, we consider again Figure 1, top. In practice the CTR foil is located inside the beam pipe with optics set up outside of the beam pipe to view and analyze the generated CTR. This is typically done through some viewing window situated on the side of the beam pipe to couple the radiation out of the vacuum.

However, if the radiated angular spectral fluence profiles is integrated out to some θ fixed by the maximum viewing angle through the window, a portion of the wavefront is suppressed. Integration over a partial solid angle yields a frequency-dependent signal suppression.

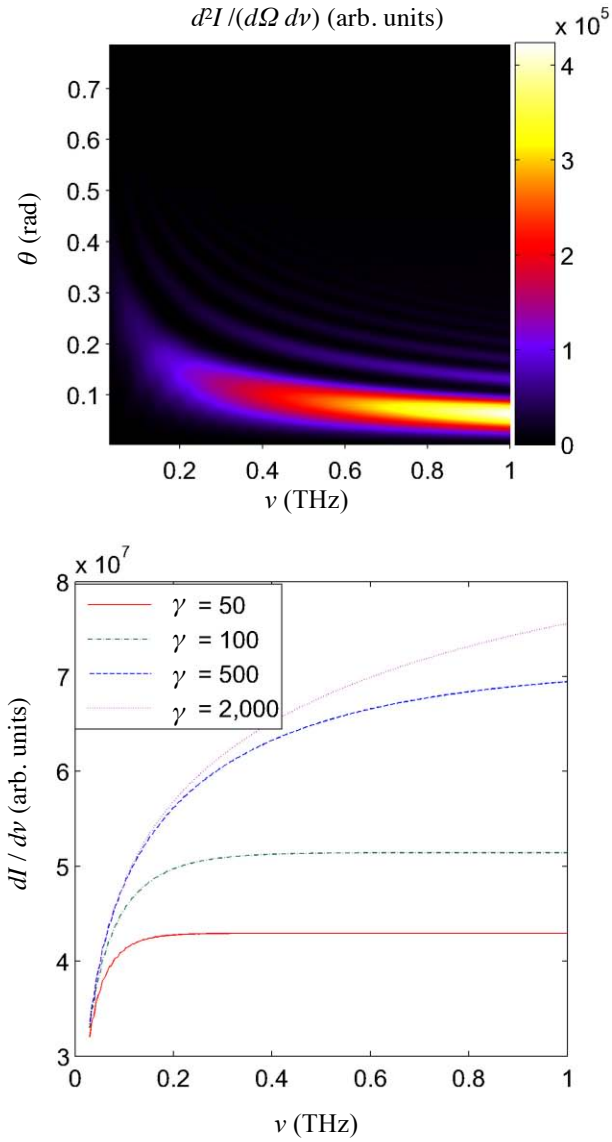

Figure 1: Angular spectral fluence profiles for TR of a γ = 100 electron at normal incidence with a 2" diameter foil at a distance of R = 2" from the center of the foil (top). Resulting emitted power spectra after integrating angular spectral fluence profiles over entire half-plane for several values of γ (bottom).

Work so far has suggested that this initial viewing window limitation as well as small final detector apertures are the typical sources for signal loss. All of these instrument-related effects are wrapped up in the response function for the system. In the computer model this is tabulated by propagating a TR wavefront through the entire instrument where it is integrated over the area of the final detecting surface. This final energy is then normalized by the total calculated input energy $I_e(\omega)$ to get a ratio of how much of the input signal survived.

The first system analyzed by the software was a Michelson interferometer. Details on its use to reconstruct the bunch form factor are presented in [7].

The resulting response curve for the device is shown in Figure 2. The flat high-frequency information still sees an overall suppression due to partial CTR wavefront acceptance at the 1" diameter quartz viewing window used to couple the CTR out of the vacuum.

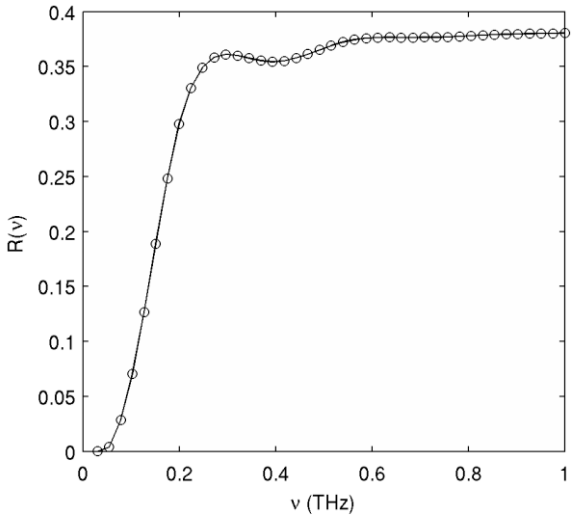

Figure 2: Response function $R(\omega)$ for the Michelson interferometer [7], including clipping at viewing window.

SIMULATED CTR-BASED BUNCH RECONSTRUCTION

Barring any dependence of the measured CTR signal on the TR strength Ie or a system response R as presented in Equation 3, one hopes to directly resolve the bunch form factor $f(\omega)$. To justify the frequency range of interest and how the results of the subsequent analyses pertain to an experimental electron beam, we have performed basic simulation of the ILC test accelerator (ILCTA) photo-injector currently under planning at Fermilab The photo-injector is composed of a radio-frequency gun followed by two TESLA-type superconducting cavities capable of accelerating the beam to approximately 50 MeV. The cavities, when ran off crest, can be used to chirp the electron bunch for longitudinal compression in a downstream magnetic chicane with momentum compaction factor R_{56} = -0.2 m. Though not comparable in energy, the typical root-mean-squared (RMS) bunch lengths under consideration also reflect projected International Linear Collider bunch lengths (σ_z = ~300μm after compression downstream of the damping rings at ~ 5 GeV).

The beam dynamics simulations of the production and low energy transport of the space-charge-dominated electron bunch was performed with ASTRA [8]. The resulting simulated 1.6 x 10^5 macroparticle bunch was used as an input in a one-dimensional, single particle longitudinal beam dynamics code. The off-crest phase of the cavity was adjusted to minimize the resulting bunch length to σ_z = 392μm (RMS).

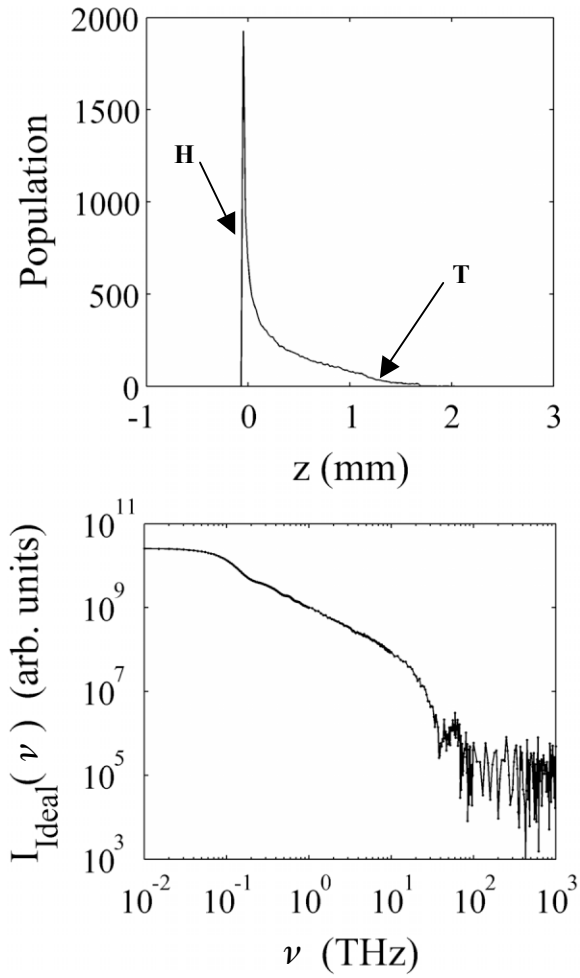

Figure 3: Simulated longitudinal bunch distribution with σ_z = 392μm (top). Corresponding ideal CTR power spectrum (bottom).

The resulting simulated longitudinal bunch distribution is shown in Figure 3 (top). Ideally, if the emitted single-electron TR and instrument had no frequency dependence, the emitted CTR power spectrum would be directly proportional to the form factor (Equation 2). This ideal power spectrum is shown on the log-log plot (Figure 3, bottom) for our modeled bunch in terms of frequency $\nu = \omega / 2\pi$. This theoretical power spectrum peaks at 2.53 x 10^{10}, just short of the expected N-squared value. The drop to incoherent noise sets in at $\nu \approx 10$ THz.

From Figure 3 we see that for a typical noisy beam, the detailed coherent spectral information on the bunch distribution lies at $\nu < 10$ THz corresponding to $\lambda > 30$μm. In principle, for a basic bunch length diagnosis, wavelengths on the order of σ_z are sufficient. For our subject bunch this corresponds to $\nu \approx 0.75$ THz.

Figure 4 shows the impact of the system response on a simulated measurement of the test bunch introduced in Figure 3. Trace A of Figure 4 is the mod-squared of the Fourier transform of the longitudinal bunch distribution, representing the ideal CTR signal [the bunch form factor $f(\omega)$]. Trace B is the corresponding spectrum that would

be measured by a detector at the end of the Michelson interferometer as calculated by Equation 3. For these calculations the detector is assumed the frequency response of the detector to be constant for all frequencies.

Figure 5 shows the equivalent bunch distributions. Shown for comparison are (A) the original bunch distribution as well as (B) the inverse discrete Fourier transform (IFDT) of $f(\omega)$. These show excellent agreement for the bunch shape for all $z > 0$, though the pathological drop of the simulated bunch is not recovered in the frequency analysis. Figure 5C shows the IFDT of the suppressed CTR signal shown in Figure 5B. This represents the bunch distribution from the suppressed signal as would be expected from experimental data.

Aside from the effective "DC offset" due to the severe zero-frequency suppression, the curve shown as Figure 5C shows little difference from the expected, noisy IFDT. While in an experiment this may be observed as a reduction in the observed tail, this can be avoided by careful analysis of the data.

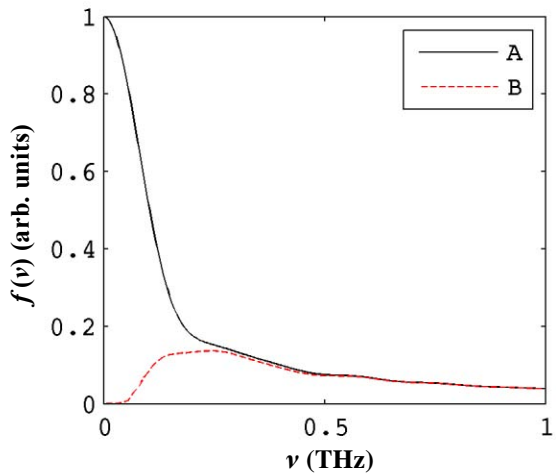

Figure 4: (A) Ideal power spectrum $f(\omega)$. (B) Simulated power spectrum $I_{measured}(\omega)$ as given by Equation 3.

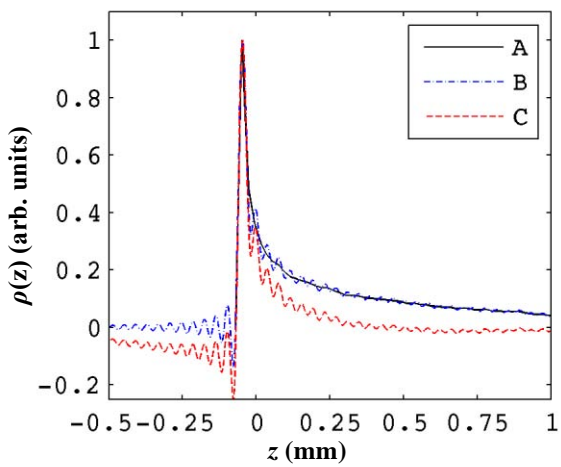

Figure 5: (A) Original bunch distribution $\rho(z)$. (B) Bunch distribution deduced by IDFT of $f(\omega)$ without phase information. (C) Bunch distribution deduced by IDFT of suppressed $f(\omega)$.

The overall qualitative agreement with the ideal signal stems from the peaked head of the bunch. The incoming longitudinal curvature results in a sharply peaked distribution with a full-width half-max (FWHM) on the order of tens of microns. Thus most of the frequency content is at frequencies higher than the characteristic frequency one would infer from the RMS value ($\omega \sim c/\sigma_z$). Comparing the FWHM values for the various bunches shows that the deduced suppressed longitudinal profile (Figure 5, trace C) is in agreement with the actual bunch profile (Figure 5, trace A) to within ~5%. This confirms that for the considered bunch distribution the critical frequencies needing to be analyzed lie in the 1 - 10 THz range where there is minimal diffraction reduction for the configuration analyzed here if the tail is of little concern.

REMARKS AND FUTURE PLANS

While this first case provided perhaps a very weak example of system response impact on longitudinal bunch diagnostics, further study is still warranted from what has been observed. Two factors minimized the expected effects including the sharply peaked longitudinal profile as well as the low beam energy. For bunches with broader bunch geometries, such as an ideal Gaussian distribution, the lower frequency information is expected to have a greater bearing on the final analysis. Furthermore, as seen in Figure 1 (bottom), higher energy bunches give $I_e(\omega)$ a frequency dependence penetrating higher into the spectrum. Early estimates show that going to 250 MeV beams roughly doubles the FWHM error of the bunch head to about 10%.

Bearing current ILC design considerations in mind, these higher energy (5 GeV downstream of the post damping ring bunch compressor) Gaussian bunch diagnostics by interferometry will be the first among upcoming analyses. Also to be studied are a very basic CTR-based phase scan device and multi-channel polychromator for single-shot bunch length estimation

REFERENCES

[1] T. Maxwell, *Diffraction Analysis of Coherent Transition Radiation Interferometry in Electron Linear Accelerators*, Master's Thesis, Northern Illinois University (2007).

[2] T.J. Maxwell, C.L. Bohn, D. Mihalcea, and P. Piot, Proceedings of 2007 IEEE Particle Accelerator Conference, 4015, Albuquerque, NM (2007).

[3] A. G. Shkvarunets and R. B. Fiorito, *Phys. Rev. Special Topics Acc. & Beams* **11**, 01281.

[4] A. S. Marathat and J. F. McCalmont, *J. Opt. Soc. Am. A.* **18**, 2585-2593 (2001).

[5] S. Casalbuoni, B. Schmidt and P. Schmüser, "Far-Infrared Transition and Diffraction Radiation", DESY Report TESLA 2005-15.

[6] T. Hahn, *Computer Science Communications* **168**, 78 (2005).

[7] D. Mihalcea, C.L. Bohn, U.Happek, and P. Piot, *Phys. Rev. Special Topics Acc. & Beams* **9**, 082801 (2006).
[8] K. Flottmann, *ASTRA: A Space Charge Tracking Algorithm,* available at http://www.desy.de/~mpyflo.